Analogy and dissimilarity of excitons in monolayer and bilayer of $MoSe_2$

2D Materials

PAPER

Analogy and dissimilarity of excitons in monolayer and bilayer of $MoSe_2$

Łucja Kipczak[1,*], Artur O Slobodeniuk[2,*], Tomasz Woźniak[3], Mukul Bhatnagar[1], Natalia Zawadzka[1], Katarzyna Olkowska-Pucko[1], Magdalena Grzeszczyk[1,4], Kenji Watanabe[5], Takashi Taniguchi[6], Adam Babiński[1] and Maciej R Molas[1,*]

[1] Institute of Experimental Physics, Faculty of Physics, University of Warsaw, 02-093 Warsaw, Poland
[2] Department of Condensed Matter Physics, Faculty of Mathematics and Physics, Charles University, CZ-121 16 Prague, Czech Republic
[3] Department of Semiconductor Materials Engineering, Wrocław University of Science and Technology, 50-370 Wrocław, Poland
[4] Institute for Functional Intelligent Materials, National University of Singapore, Singapore 117544, Singapore
[5] Research Center for Functional Materials, National Institute for Materials Science, Tsukuba 305-0044, Japan
[6] International Center for Materials Nanoarchitectonics, National Institute for Materials Science, Tsukuba 305-0044, Japan
[*] Authors to whom any correspondence should be addressed.

E-mail: lucja.kipczak@fuw.edu.pl, aslobodeniuk@karlov.mff.cuni.cz and maciej.molas@fuw.edu.pl

OPEN ACCESS

RECEIVED
29 November 2022

REVISED
2 February 2023

ACCEPTED FOR PUBLICATION
16 February 2023

PUBLISHED
28 February 2023

Keywords: monolayer MoSe2, bilayer MoSe2, excitons, binding energy, DFT calculations, kp approach, g-factor

Supplementary material for this article is available online

Abstract

Excitons in thin layers of semiconducting transition metal dichalcogenides are highly subject to the strongly modified Coulomb electron–hole interaction in these materials. Therefore, they do not follow the model system of a two-dimensional hydrogen atom. We investigate experimentally and theoretically excitonic properties in both the monolayer (ML) and the bilayer (BL) of $MoSe_2$ encapsulated in hexagonal BN. The measured magnetic field evolutions of the reflectance contrast spectra of the $MoSe_2$ ML and BL allow us to determine g-factors of intralayer A and B excitons, as well as the g-factor of the interlayer exciton. We explain the dependence of g-factors on the number of layers and excitation state using first principles calculations. Furthermore, we demonstrate that the experimentally measured ladder of excitonic s states in the ML can be reproduced using the $\mathbf{k}\cdot\mathbf{p}$ approach with the Rytova–Keldysh potential that describes the electron–hole interaction. In contrast, the analogous calculation for the BL case requires taking into account the out-of-plane dielectric response of the $MoSe_2$ BL.

1. Introduction

The optical response of monolayers (MLs) belonging to semiconducting transition metal dichalcogenides (S-TMDs), such as MoS_2, $MoSe_2$, $MoTe_2$, WS_2, and WSe_2, is dominated by the excitonic emission/absorption even at room temperature [1–4]. This is due to the binding energies (BEs) of excitons, i.e. bound electron–hole (e-h) pairs, which are as large as a few hundred meV [5–9]. The most unconventional property of these excitons is their non-Rydberg model spectrum, which cannot be described by the standard two-dimensional (2D) hydrogen atom [10, 11]. A typical approach to account for the excitonic spectra of S-TMD MLs refers to the numerical solutions of the Schrödinger equation, in which the e-h attraction is approximated by the Rytova–Keldysh (RK) potential [12, 13]. Although this is a well-known method for the ML, the corresponding analysis of the excitonic ladder for the bilayer (BL) has not been reported so far.

Moreover, the electronic bands in a BL and other 2 H-stacked multilayers, are known to be effectively modified compared to the ML case [4, 14–18]. This, in particular, implies the indirect bandgap in multilayers, which strongly affects their emission spectra [1–4]. Instead, more subtle effects of the hybridisation of electronic states around the direct bandgap in multilayers are relevant for absorption-type processes [17, 19, 20]. Recently, it has been shown that the absorption resonances due to the interlayer/hybridised excitons observed in the bi- and trilayers of S-TMDs can be widely tuned using the external electric field applied perpendicularly to the layers

plane [18, 21–26], which understanding may be also of importance in potential applications.

The external out-of-plane magnetic field is widely applied to study the thin layers of S-TMDs due to their significant Zeeman response [27, 28]. Consequently, the measured emission/absorption resonances split into two circularly polarised components with the magnitude of the Zeeman splitting denoted by the g-factor. Because of the g-factor values found in S-TMD MLs, different types of transition can be identified: bright (g-factor about -4), spin- (-8) and momentum-forbidden dark (-12) [29–32]. In the case of BL, the found g-factors are more scattered. As for intralayer excitons in S-TMD BLs, the found g-factors are also about -4 [27, 28, 33], the corresponding g-factors for interlayer excitons are around 8 [17]. Then, the g-factor not only gives us information concerning the Zeeman effect, but can also be a method to identify different excitonic complexes in thin layers of S-TMDs.

In this work, we investigate experimentally and theoretically excitonic properties in high-quality ML and BL of molybdenum diselenide ($MoSe_2$) encapsulated in hexagonal boron nitride (hBN). The low-temperature ($T = 10$ K) reflectance contrast (RC) spectra are measured in external magnetic fields up to 10 T, applied in the out-of-plane configuration. Resonances, related to both neutral A and B excitons, are identified in ML and BL. Moreover, the transition associated with the interlayer exciton (IL) was recognised in the RC spectra of BL. The excitation ladder of A excitons in the ML and BL limits is modelled based on the $\mathbf{k}\cdot\mathbf{p}$ approach using the modified RK potential. Furthermore, the experimentally obtained Landé g-factors of the excitonic resonances are explained by first principles calculations. Apart from the Introduction and Summary sections, our paper is composed of three (2–4) main sections completed by the Methods section and the supplemental material (SM). First, in section 2, we focus on the analysis of the magnetic field evolutions of the RC spectra measured on the $MoSe_2$ ML and BL. The theoretical approach for excitation spectra of excitons in the S-TMD ML and BL using the $\mathbf{k}\cdot\mathbf{p}$ method is presented in section 3. Section 4 is dedicated to calculations of the excitonic g-factors in the $MoSe_2$ ML and BL.

2. Experimental results

Figures 1(a) and (b) present the RC spectra measured on the ML and BL of $MoSe_2$ encapsulated in hBN at the selected values of applied out-of-plane magnetic fields. The two main resonances, labelled correspondingly $1s^A$ and $1s^B$ in the figure, are associated with the absorption processes of the ground s states of the intralayer A and B excitons [3, 6]. The appearance of the A and B excitons is due to a relatively large spin-orbit splitting in the $MoSe_2$ VB [6]. For the ML, the first excited s state of the A exciton ($2s^A$) is also observed with a substantially lower intensity compared to the main $1s^A$ and $1s^B$ resonances. There are two less pronounced transitions apparent in the RC spectra measured on the BL, denoted $2s^A$ and IL, which we attribute correspondingly to the first excited state of the A exciton and to the interlayer exciton. The identification of the $1s^A$, $1s^B$, and $2s^A$ resonances, observed in the RC spectrum of the $MoSe_2$ ML, is straightforward and is in accordance with many other studies on $MoSe_2$ MLs encapsulated in hBN [8, 9, 34]. The measured low-temperature RC spectrum of the $MoSe_2$ BL is similar to that reported in [19].

As can be appreciated from figure 1, all the observed resonances split into two circularly polarised components under the applied out-of-plane magnetic field due to the Zeeman effect [27]. The intralayer A- and B-related resonances are characterised by the same sign of the splitting (σ^+ energy is lower than the σ^- one), but with different magnitude. At the same time, the splitting of the IL transition is opposite (σ^- energy is lower than σ^+ one). In order to investigate in detail the magnetic field evolution of the observed resonances, we fitted them using the Fano-type function. As we have not performed the analysis within the framework of the transfer matrix method combined with the Lorentz oscillator model [4], the extracted energy evolutions as a function of magnetic field are biased, particularly, for the resonances with small intensity ($2s^A$, IL). A detailed description of the A, B and IL excitons, and their optical selection rules in terms of the electronic band structure can be found in the SM.

The field evolution for the $\sigma^\pm$ components of the investigated transitions is presented in figure 2. Upon application of an out-of-plane magnetic field (B), the magnetic-field dependences of the $\sigma^\pm$ energies ($E_{\sigma^\pm}$) can be defined as $E_{\sigma^\pm}(B) = E_0 \pm 1/2 g\mu_B B$, where E_0 is the transition energy at zero field, g denotes the g-factor of the considered resonance, μ_B is the Bohr magneton. The fitted curves are presented in figure 2. The E_0 energies and the g-factors for all the studied transitions are summarised in table 1. To verify the obtained values of the g-factors, we also calculate theoretically the corresponding g-factors using the density functional theory (DFT) method, see section 4 for details. The experimentally determined g-factors for the ground states of the A (B) excitons, i.e. $1s^A$ ($1s^B$), in the ML and BL of $MoSe_2$ equal to -3.91 ± 0.10 (-4.27 ± 0.17) and -2.94 ± 0.22 (-2.77 ± 0.34), respectively. These values agree very well with those theoretically calculated (see table 1) and those previously reported for the intralayer A and B excitons in the $MoSe_2$ ML and BL [9, 27, 28, 33]. The g-factors found for the first excited states ($2s^A$) of the A exciton in both ML and BL are -4.99 ± 0.34 and -4.32 ± 0.49, respectively. It is interesting that the magnitudes of the $2s$$g$-factors are significantly

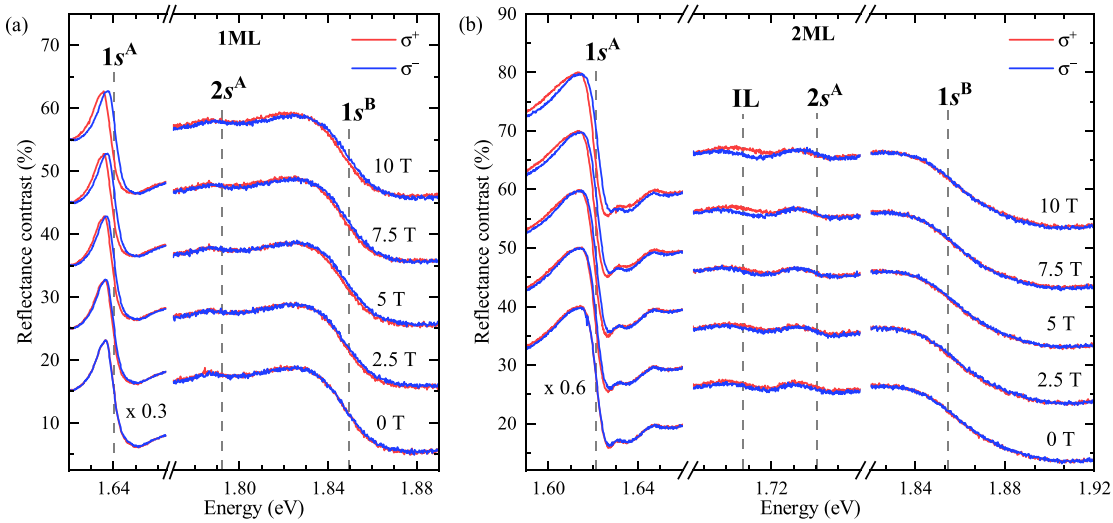

Figure 1. Helicity-resolved RC spectra of (a) monolayer and (b) bilayer of $MoSe_2$ encapsulated in hBN for selected values of magnetic field measured at $T = 10$ K. The red and blue curves correspond to σ^+ and σ^- polarizations of reflected light in magnetic fields applied perpendicularly to the layers plane, respectively. The spectra are vertically shifted for clarity.

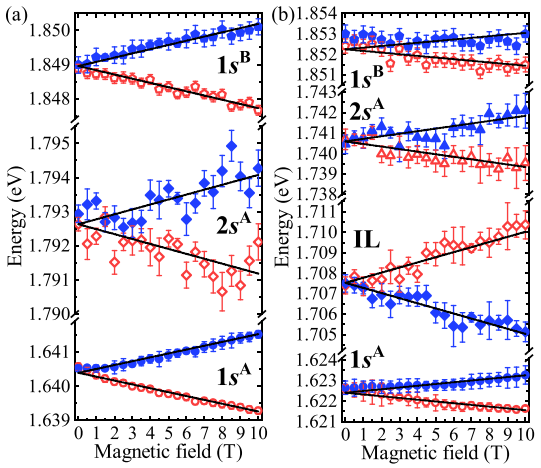

Figure 2. Obtained excitonic energies of the $\sigma^{\pm}$ components of the transitions measured on (a) monolayer and (b) bilayer of $MoSe_2$ encapsulated in hBN as a function of the out-of-plane magnetic field. The red and blue points correspond to σ^+ and σ^- polarizations, respectively. The solid black lines represent fits according to the equation described in the text.

Table 1. Experimentally determined values of the E_0 energies and the g-factors for all the studied transitions. The g^{calc} values correspond to the theoretically calculated parameters using DFT method. Notably, the experimental values of the E_0 energy and the g-factor are assumed to be obtained for the IL^A exciton.

	E_0	g	g^{calc}
	monolayer		
$1s^A$	1.640 ± 0.001	-3.91 ± 0.10	-3.69
$2s^A$	1.793 ± 0.005	-4.99 ± 0.34	-3.90
$1s^B$	1.849 ± 0.003	-4.27 ± 0.17	-3.75
	bilayer		
$1s^A$	1.622 ± 0.001	-2.94 ± 0.22	-3.00
$2s^A$	1.741 ± 0.006	-4.32 ± 0.49	-3.19
$1s^B$	1.852 ± 0.003	-2.77 ± 0.34	-3.16
$IL^{A/B}$	1.708 ± 0.006	$+8.62 \pm 0.42$	$+8.71/+8.91$

larger (of about $30\% - 50\%$) than those of the $1s^A$ states. In contrast, the theoretically calculated values of the g-factors for the $1s$ and $2s$ states of the A excitons are larger by about a few percent. Both possible changes (i.e. increase or decrease) of the corresponding g-factors of the s states are reported in the literature [8, 9, 35–38]. In our opinion, the discrepancy between the experimental and theoretical values of the $2s^A$ g-factor requires a more sophisticated analysis, which goes beyond the scope of this work. The value of g-factor for the IL transition of 8.62 ± 0.42, which has not been reported so far, is in very good agreement with the theoretically calculated values of 8.71 and 8.91 for the IL^A and IL^B excitons, respectively. As the IL^A resonance is reported mainly in MoS_2 and $MoSe_2$ BLs [17–20, 26, 39, 40], we ascribe the observed IL resonance to the IL^A. Further discussion on the interlayer excitons can be found in the SM.

3. Excitonic ladder in ML and BL: theoretical approach

A common approach to account for the excitation spectra of excitons in S-TMD MLs refers to the numerical solutions of the Schrödinger equation, in which the e-h attraction is approximated by RK potential [12, 13]. Although this numerical method gives very good results for Mo- and W-based MLs [9, 35, 41], there is a lack of analogous calculations of the excitation spectra of excitons in multilayer systems (particularly, in a BL). In the following, the

calculations of the excitonic ladders of the s states in both the ML and the BL of the S-TMDs are presented. In order to verify our theoretical results, we compare them with the experimentally found energy separation between the 1s and 2s states, $\Delta E_{12}^{\mathrm{exp}}$, obtained using the values shown in table 1. Our comprehensive approach to the theoretical analysis of the excitation spectra of excitons in S-TMD ML and BL is described in detail in the SM.

First, we calculate a spectrum of the intralayer excitons in the ML and BL with the help of the effective two-body hydrogen-like problem. We derive such a problem from the band Hamiltonians of the considered 2D systems within the $\mathbf{k}\cdot\mathbf{p}$ approximation. To do this, we first consider the basic electronic properties of S-TMD ML. The ML crystal is a direct bandgap semiconductor. The extrema of the valence (VB) and conduction (CB) bands are located at the $\mathrm{K}^{\pm}$ points of the Brillouin zone (BZ). Due to the strong spin-orbit interaction, both bands are spin-split. The values of the splittings in the VB (Δ_v) and in the CB (Δ_c) are hundreds and tens of meV, respectively [42]. Therefore, the Bloch states at the K points can be presented as a tensor product of the spin $\{|\downarrow\rangle, |\uparrow\rangle\}$ and the spinless band states. The spinless VB and CB states at $\mathrm{K}^{\pm}$ points are made predominantly from $d_{x^2-y^2} \pm id_{xy}$ and d_{z^2} orbitals of transition metal atoms, respectively [42, 43]. Such a structure of Bloch states in opposite K points defines the optical selection rules in the ML and is a consequence of the system's time-reversal symmetry (TRS). The TRS also dictates that Bloch states with the same band index (c or v) but with opposite spins in opposite valleys have equal dispersion laws, i.e. the same band structure. Therefore, we restrict our consideration of the conduction and valence bands to the K^{+} point for brevity. All conclusions for the K^{-} point can be done by analogy.

The A excitons at the K^{+} point of the ML are formed from an electron from the bottom spin-up CB and a hole from the top spin-up VB. The corresponding spinless Bloch functions are $|\Psi_c\rangle$ and $|\Psi_v\rangle$. The two-band fully-diagonalized Hamiltonian of these bands, written in the corresponding basis $\{|\Psi_c\rangle \otimes |\uparrow\rangle, |\Psi_v\rangle \otimes |\uparrow\rangle\}$, can be presented in the form [44]

$$H_{\mathrm{ML}} = \begin{bmatrix} E_g + \frac{\hbar^2\mathbf{k}^2}{2m_e} & 0 \\ 0 & -\frac{\hbar^2\mathbf{k}^2}{2m_h} \end{bmatrix}. \qquad (1)$$

Here, E_g is the bandgap energy parameter, $\mathbf{k} = k_x\mathbf{e}_x + k_y\mathbf{e}_y$ is the in-plane momentum of the quasiparticles in the ML, where $\mathbf{e}_x, \mathbf{e}_y$ are unit vectors in the x and y directions, respectively. $m_e, m_h > 0$ are correspondingly the electron and hole effective masses in the ML. The Rydberg-type spectrum of e-h pairs for such a band structure can be found from the solution of the corresponding eigenvalues problem [13, 45]

$$\left\{-\frac{\hbar^2}{2\mu}\nabla_{\parallel}^2 + V_{\mathrm{RK}}(\rho)\right\}\psi(\rho) = E\psi(\rho), \qquad (2)$$

where $\mu = m_e m_h/(m_e + m_h)$ is the reduced exciton mass, $\nabla_{\parallel} = \mathbf{e}_x\partial_x + \mathbf{e}_y\partial_y$ is the 2D nabla operator, ρ is the in-plane distance between an electron and a hole of the exciton, E is the exciton energy, and $V_{RK}(\rho)$ is the Rytova–Keldysh potential [12, 13]

$$V_{\mathrm{RK}}(\rho) = -\frac{\pi e^2}{2r_0}\left[\mathrm{H}_0\left(\frac{\rho\varepsilon}{r_0}\right) - Y_0\left(\frac{\rho\varepsilon}{r_0}\right)\right]. \qquad (3)$$

Here $\mathrm{H}_0(x)$ and $Y_0(x)$ correspond to the Struve and Bessel functions of the second kind, $r_0 = 2\pi\chi_{2D}$ represents the screening length, χ_{2D} is the ML 2D polarizability [41, 46]. ε denotes the dielectric constant of the surrounding medium (hBN in our study).

Let us consider the band structure of the BL at the K^{+} point. To do this, we first define the Bloch states of the VB and CB at the K^{+} point of the BL, by constructing them from the ML Bloch states of the top and bottom layers of the BL. Namely, we introduce the states $|\Psi_n^{(m)}\rangle \otimes |s\rangle$, where $m = 1, 2$ is a layer index (for bottom and top layers, respectively), $n = v, c$ is a band index (for VB and CB) and $s = \uparrow, \downarrow$ specifies the spin degree of freedom. The bottom (first) layer states $|\Psi_v^{(1)}\rangle$ and $|\Psi_c^{(1)}\rangle$ are made predominantly from $d_{x^2-y^2} + id_{xy}$ and d_{z^2} orbitals of transition metal atoms, respectively [42, 43]. They coincide with ML spinless states $|\Psi_v\rangle$ and $|\Psi_c\rangle$, considered above. The top (second) layer states $|\Psi_v^{(2)}\rangle$ and $|\Psi_c^{(2)}\rangle$ are made from $d_{x^2-y^2} - id_{xy}$ and d_{z^2} orbitals and coincide with spinless states in the K^{-} point of the ML. In our study, we suppose the orthogonality of the basis states from different layers and bands $\langle\Psi_n^{(m)}|\Psi_{n'}^{(m')}\rangle = \delta_{nn'}\delta_{mm'}$.

The symmetry analysis of the BL system [17, 28, 40] demonstrates that the electron excitations of the CB of the different layers do not interact with each other in the leading order, i.e. the electron states of the BL are localised either in the bottom or in the top layer. On the contrary, the VB of the different layers of the BL interact with each other forming the new VB with the Bloch states delocalised in the out-of-plane direction. These states can be found by diagonalizing the VB part of the BL Hamiltonian, written on the basis $\{|\Psi_v^{(1)}\rangle \otimes |\uparrow\rangle, |\Psi_v^{(2)}\rangle \otimes |\uparrow\rangle, |\Psi_v^{(2)}\rangle \otimes |\downarrow\rangle, |\Psi_v^{(1)}\rangle \otimes |\downarrow\rangle\}$

$$H_{\mathrm{BL}}^{\mathrm{VB}} = \begin{bmatrix} -\frac{\hbar^2\mathbf{k}^2}{2m_h} & t & 0 & 0 \\ t & -\Delta_v - \frac{\hbar^2\mathbf{k}^2}{2m_h} & 0 & 0 \\ 0 & 0 & -\frac{\hbar^2\mathbf{k}^2}{2m_h} & t \\ 0 & 0 & t & -\Delta_v - \frac{\hbar^2\mathbf{k}^2}{2m_h} \end{bmatrix}, \qquad (4)$$

where t is the interlayer hopping term. The spectrum of this Hamiltonian is doubly degenerated by spin (in full accordance with the TRS and inverse symmetry of the BL)

$$E_{\mathrm{VB}}^{\pm} = -\frac{\hbar^2\mathbf{k}^2}{2m_h} - \frac{\Delta_v}{2} \pm \sqrt{\frac{\Delta_v^2}{4} + t^2}. \qquad (5)$$

The eigenstates that correspond to the upper-energy E^{+}_{VB} bands are

$$|\Phi^{+}_{v\uparrow}\rangle = \left[\cos\theta|\Psi^{(1)}_{v}\rangle + \sin\theta|\Psi^{(2)}_{v}\rangle\right]\otimes|\uparrow\rangle, \quad (6)$$

$$|\Phi^{+}_{v\downarrow}\rangle = \left[\sin\theta|\Psi^{(1)}_{v}\rangle + \cos\theta|\Psi^{(2)}_{v}\rangle\right]\otimes|\downarrow\rangle, \quad (7)$$

where we introduced $\cos(2\theta) = \Delta_v/\sqrt{\Delta_v^2 + 4t^2}$. It is important to point out that the new Bloch states describe the delocalised in the out-of-plane direction VB excitations. For example, the state $|\Phi^{+}_{v\uparrow}\rangle$ describes the VB excitation, which can be found with probabilities $P^{(1)} = \cos^2\theta$ and $P^{(2)} = \sin^2\theta$ in the first (bottom) and second (top) layers, respectively. The eigenstates $|\Phi^{-}_{v\uparrow}\rangle$ and $|\Phi^{-}_{v\downarrow}\rangle$, which correspond to the lower-energy E^{-}_{VB} bands, can be derived from the first ones by replacing $\cos\theta \to -\sin\theta, \sin\theta \to \cos\theta$.

The optical transitions in the K^{+} point of the BL, which form the intralayer A-excitons in the BL, couple either $\{|\Psi^{(1)}_{c}\rangle\otimes|\uparrow\rangle, |\Phi^{+}_{v\uparrow}\rangle\}$ or $\{|\Psi^{(2)}_{c}\rangle\otimes|\downarrow\rangle, |\Phi^{+}_{v\downarrow}\rangle\}$ group of the bands. The transitions between the first pair of the bands are active in σ^{+} polarised light, while the transitions between the second pair of the bands are active in σ^{-} polarised light. The first and second groups of the bands are described by the same Hamiltonian

$$H_{\mathrm{BL}} = \begin{bmatrix} E_g + \frac{\hbar^2\mathbf{k}^2}{2m_e} & 0 \\ 0 & -\frac{\hbar^2\mathbf{k}^2}{2m_h} - \frac{\Delta_v}{2} + \sqrt{\frac{\Delta_v^2}{4} + t^2} \end{bmatrix}, \quad (8)$$

which looks similar to the two-band Hamiltonian of the ML, compare with equation (1). The effective electron and hole masses of these bands coincide with the corresponding masses in the ML (in the leading order of the $\mathbf{k}\cdot\mathbf{p}$ approximation). Therefore, the intralayer A-excitons are characterised by the same reduced mass μ, as in the ML. On the other hand, the delocalisation of the VB Bloch state in the out-of-plane direction leads to the modification of the Coulomb interaction between such a hole excitation and an electron excitation, which remains localised in one of the layers. The modified Coulomb interaction in the BL $V_{\mathrm{bil}}(\rho)$ is derived in the SM. In summary, we conclude that the spectrum of the intralayer A-excitons can be derived from equation (2) by replacing $V_{\mathrm{RK}}(\rho)$ with $V_{\mathrm{bil}}(\rho)$.

3.1. ML

We derive the spectrum of excitons in the ML by solving equation (2) with Rytova–Keldysh potential (3). Following, we introduce the dimensionless parameters $\xi = \rho\varepsilon/r_0$ and $\epsilon = E/Ry^*$, with $Ry^* = \mu e^4/2\hbar^2\varepsilon^2$ and rewrite equation (2) for the case of s-type excitons in the following form

$$\left\{b^2\frac{1}{\xi}\frac{d}{d\xi}\left(\xi\frac{d}{d\xi}\right) + bv_{\mathrm{RK}}(\xi) + \epsilon\right\}\psi(\xi) = 0, \quad (9)$$

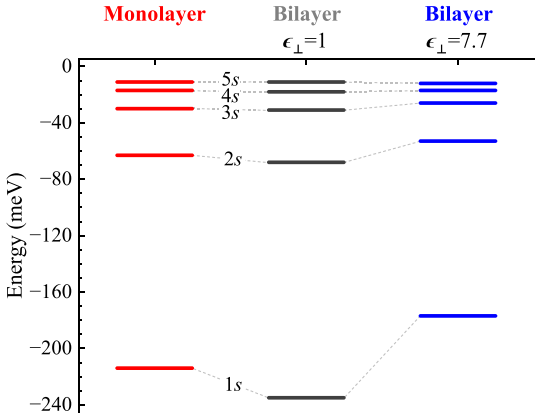

Figure 3. Energy spectrum of s excitonic state of the $MoSe_2$ ML and BL encapsulated in hBN calculated using the $\mathbf{k}\cdot\mathbf{p}$ approach. The $\epsilon_\perp$ parameter denotes the out-of-plane dielectric constant used in calculations.

where $b = \hbar^2\varepsilon^2/\mu e^2 r_0$ and $v_{\mathrm{RK}}(\xi) = \pi[\mathrm{H}_0(\xi) - Y_0(\xi)]$. The parameter Ry^* defines the natural energy scale for the considered excitonic problem, see [8] for details. The dimensionless parameter b is the ratio of the reduced Bohr radius $a_0^* = \hbar^2\varepsilon/\mu e^2$ and the reduced screening length $r_0^* = r_0/\varepsilon$ in the system. We use $\varepsilon = 4.5$ [47], $r_0 = 51.7$ Å, $\mu = 0.44m_0$ for our calculations, yielding $b \approx 0.47$, see details in the SM. The numerical solution of the equation for this value of b gives the energies of the ground ($1s$) and the first four excited ($2s$, $3s$, $4s$, and $5s$) states equal to $E_1 = -214$ meV, $E_2 = -63$ meV, $E_3 = -30$ meV, $E_4 = -17$ meV, $E_5 = -11$ meV, respectively. The calculated energy positions of the excitonic states in ML are presented in figure 3. It is difficult to predict the absolute energy of a given ns excitonic state, $E_{n,ex} = E_{\mathrm{g}} + E_n$, since the bandgap energy (E_{g}) is renormalised by the Coulomb interaction and also depends on the dielectric constant ε. Calculating such a bandgap shift requires an additional more resource-demanding numerical investigation. To verify our theoretical calculations, we determine the energy distance between $1s$ and $2s$ emission lines $\Delta E_{12} = E_{1,ex} - E_{2,ex} = (E_{\mathrm{g}} + E_1) - (E_{\mathrm{g}} + E_2)$. Therefore, we found $|\Delta E_{12}| = 151$ meV, which is nearly perfectly consistent with our experimental value $|\Delta E_{12}^{\mathrm{exp}}| = 153 \pm 5$ meV as well as the previously reported value of about 153 meV obtained from photoluminescence experiment [8].

3.2. BL

The computation of the excitonic spectrum in the BL of S-TMDs is a much more sophisticated task. For the ML case, the charges and wavefunctions of an electron and a hole are confined within the ML plane. The situation with the electron and hole electronic excitations in the BL is more complex. The hybridisation of the VB states leads to the charge redistribution of hole quasiparticles between layers in the BL [4, 17, 40]. Using the properties of the VB states in

the BL, we obtain the following values for the charges of the hole excitation, which belong to the same ($Q_{\rm in}$) and opposite ($Q_{\rm opp}$) layers as an electron,

$$Q_{\rm in/opp} = \frac{|e|}{2}\left(1 \pm \frac{\Delta_v}{\sqrt{\Delta_v^2 + 4t^2}}\right) \approx 0.932|e|/0.068|e|, \tag{10}$$

where '+' and '−' signs correspond to the same (in) and opposite (opp) layers of the BL, respectively. Here we used the numbers $\Delta_v = 182$ meV and $t = 53$ meV [43]. Subsequently, the redistribution of the hole charge in the out of-plane-direction modifies the Coulomb potential between electron and hole excitations in the BL. The derivation of the corresponding potential $V_{\rm bil}(\rho)$ as a function of the in-plane distance, ρ between an electron and hole excitation is presented in the SM. The potential $V_{\rm bil}(\rho)$ depends on the distance L between the layers in the BL, the screening length r_0, the dielectric constant of the medium surrounding the BL ε, and finally the out-of-plane dielectric constant $\epsilon_\perp$ of the BL. The case $\epsilon_\perp = 1$ corresponds to the limit situation when the BL can not be polarised by an electric field in an out-of-plane direction. In the real situation the BL, however, may be characterised by the out-of-plane dielectric constant $\epsilon_\perp$, which is different from unity $\epsilon_\perp = \epsilon_\perp^{\rm bil} > 1$. In the following, we demonstrate that the first case can not explain the experimental observables, and hence, it confirms that the BL is polarised in an out-of-plane direction.

Let us consider the case $\epsilon_\perp = 1$. Then, the excitonic spectrum of the s states can be calculated using the dimensionless eigenvalue equation (with the same notations for ε and b from the previous section)

$$\left\{b^2 \frac{1}{\xi}\frac{d}{d\xi}\left(\xi\frac{d}{d\xi}\right) + b\nu_{\rm bil}(\xi) + \epsilon\right\}\psi(\xi) = 0, \tag{11}$$

with the dimensionless electrostatic potential between an electron and a hole in the BL

$$\nu_{\rm bil}(\xi) = 2\varepsilon\int_0^\infty dx J_0(x\xi)\frac{0.932(1-\delta)\left(e^{2xl}[(1-\delta)\varepsilon x+1] - [\varepsilon x(1-\delta)+\delta]\right) + (0.0681-\delta)^2 e^{xl}}{e^{2xl}[(1-\delta)\varepsilon x+1]^2 - [\delta+\varepsilon x(1-\delta)]^2}. \tag{12}$$

Here, $J_0(x)$ is the Bessel function of the first kind, $\delta = (\varepsilon-1)/(\varepsilon+1) \approx 0.64$, and $l = L\varepsilon/r_0 \approx 0.56$. In the latter, we used $L = 6.44$Å for $MoSe_2$ BL from HQ Graphene. The $\nu_{\rm bil}(\xi)$ potential is composed of two components: intra- (the term with 0.932 multiplier) and interlayer (the term with 0.068 multiplier). One can see that the intralayer term is dominant at a large l distance between the layers, whereas the contribution of the interlayer term decays exponentially with this distance $\propto \exp(-xl)$. Using numerical solution of the eigenvalue problem with potential $\nu_{\rm bil}(\xi)$, we obtain $E_1 = -235$ meV, $E_2 = -68$ meV, $E_3 = -31$ meV, $E_4 = -18$ meV, and $E_5 = -11$ meV. The calculated energy positions of the excitonic states in the BL are presented in figure 3. The obtained BEs of the consecutive s excitons in the BL are slightly larger compared to their ML counterparts. This can be explained by the fact that the effective dielectric constant for the BL is smaller than that for the ML case. However, the calculated difference between the energies of the 1s and 2s excitons, $|\Delta E_{12}| = 167$ meV, is significantly larger as compared to the experimental value, $|\Delta E_{12}^{\rm exp}| = 119 \pm 6$ meV. Therefore, the model with an out-of-plane dielectric constant, $\epsilon_\perp = 1$ fails in the BL.

Consequently, we calculate the excitonic spectrum in the BL assuming that $\epsilon_\perp = 7.7$ [48], which is the value that describes the static dielectric constant in the $MoSe_2$ BL [48]. The resulting eigenvalue equation in dimensionless coordinate $\xi = \rho\varepsilon\sqrt{\epsilon_\perp}/r_0$ becomes

$$\left\{b^2\epsilon_\perp \frac{1}{\xi}\frac{d}{d\xi}\left(\xi\frac{d}{d\xi}\right) + b\widetilde{\nu}_{\rm bil}(\xi) + \epsilon\right\}\psi(\xi) = 0, \tag{13}$$

with the new electrostatic potential, $\widetilde{\nu}_{\rm bil}(\xi)$, which is obtained from equation (12) by replacing $\delta \to \widetilde{\delta} = (\varepsilon - \sqrt{\epsilon_\perp})/(\varepsilon + \sqrt{\epsilon_\perp}) \approx 0.24$. The dimensionless energy parameter remains the same as in the previous case. The eigenvalues of this new equation provide the following spectrum of excitons $E_1 = -177$ meV, $E_2 = -53$ meV, $E_3 = -26$ meV, $E_4 = -17$ meV, and $E_5 = -12$ meV. The calculated energy positions of the excitonic states in the BL with $\epsilon_\perp = 7.7$ are presented in figure 3. Consequently, the new energy separation $|\Delta E_{12}| = 124$ meV agrees nicely with the experimental value ($|\Delta E_{12}^{\rm exp}| = 119 \pm 6$ meV).

To conclude, we demonstrate that the excitation spectrum of excitons in the $MoSe_2$ ML can be properly reproduced using the RK potential with the approach of infinitely thin ML. However, the Rytova–Keldysh potential can not be applied to describe the spectrum of the intralayer excitons in the BL as a result of the more complex structure of the BL crystal. We derive the electrostatic potential in the BL by taking into account the geometry and the dielectric constant $\epsilon_\perp$ of the BL perpendicular to the layers' planes. The spectrum of excitons, based on the new

potential in the $MoSe_2$ BL is in very good agreement with the experimental data. Our results indicate that the study of excitons in thin layers of S-TMDs, beyond the ML limit, is much more complicated and requires taking into account a realistic thickness of the BL and its dielectric response.

4. *g*-factors of exciton *ns* states

The *g*-factors of excitonic *ns* states, g^X_{ns}, can be calculated using the dispersions of the band-to-band transitions, $g^X(\mathbf{k})$, in the vicinity of the K^+ point, along with the exciton wave functions, $|\psi^X_{ns}(\mathbf{k})|$ (obtained from our aforementioned $\mathbf{k}\cdot\mathbf{p}$ calculations), following [36]

$$g^X_{ns} = \int_{\mathbf{k}} |\psi^X_{ns}(\mathbf{k})|^2 g^X(\mathbf{k}) \mathrm{d}\mathbf{k} \tag{14}$$

with

$$g^X(\mathbf{k}) = \pm 2(g_{c(+1)}(\mathbf{k}) - g_{v(-1)}(\mathbf{k})), \tag{15}$$

where the sign is defined by the optical selection rules at $K^{\pm}$ points. $g_{c(+1)}(\mathbf{k})$ and $g_{v(-1)}(\mathbf{k})$ are the *g*-factors of the spin-split subbands (Bloch states), $|m\mathbf{k}\rangle$, involved in the excitonic transition, evaluated as

$$g_m(\mathbf{k}) = L^z_m(\mathbf{k}) + S^z_m(\mathbf{k}). \tag{16}$$

The *z* component of the orbital angular momentum of a Bloch state is calculated from the bands–summation formula [49]

$$L^z_m(\mathbf{k}) = \frac{1}{im_0} \sum_{l=1, l\neq m}^{N} \frac{p^x_{ml}(\mathbf{k}) p^y_{lm}(\mathbf{k}) - p^y_{ml}(\mathbf{k}) p^x_{lm}(\mathbf{k})}{\varepsilon_m(\mathbf{k}) - \varepsilon_l(\mathbf{k})}, \tag{17}$$

where m_0 is the free electron mass, $p^{x,y}_{ml}(\mathbf{k})$ are components of the momentum operator matrix elements, $\varepsilon_m(\mathbf{k})$ are the band energies, and the summation runs over all *N* states in the basis set. The elements $p^{x,y}_{ml}(\mathbf{k})$ were obtained from density perturbation theory calculations [50]. In order to converge $L^z_m(\mathbf{k})$ up to 0.1, 480 bands per formula unit were taken into account. The spin angular momentum $S^z_m(\mathbf{k}) = \pm 1$ for the considered bands. We would like to emphasize that the calculated values of the band *g*-factors for spin-orbit split subbands at the $K^{\pm}$ points are discussed in the SM.

The calculated exciton wave functions squared (see the SM for details) and *g*-factor dispersions in *k*-space around K^+ point, that enter equation (14), are presented in figure 4. The widths of the wave functions of the A and B excitons are similar in ML and BL, with a greater spread of $|\psi^B_{1s}(\mathbf{k})|^2$ than $|\psi^A_{1s}(\mathbf{k})|^2$, due to a larger effective mass of the B exciton. The opposite is observed for the interlayer excitons. The $g^X(\mathbf{k})$ dependence has a positive curvature in both the ML and BL structures, with a smaller $|g^X(\mathrm{K})|$ in BL. This is caused by the reduction of the bands *g*-factors in BL versus ML (see the SM). As a result, the magnitudes of g^X_{ns} in BL are reduced with respect to ML. Furthermore, a stronger localisation of the $2s^A$ state around the K point leads to the increase of their *g*-factor magnitudes, in agreement with previous theoretical and experimental findings [36, 38]. Due to the different signs of valence and conduction Bloch states *g*-factors involved in IL^A and IL^B excitons, their *g*-factors are positive and exhibit a negative curvature.

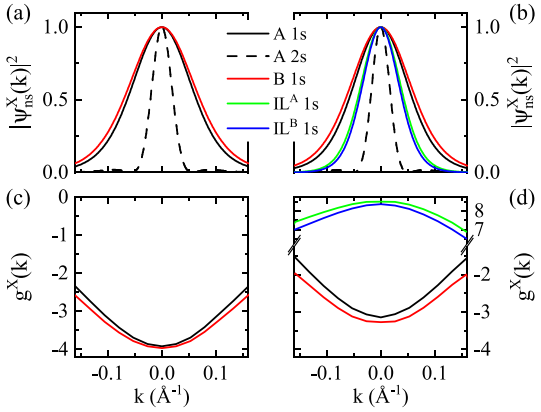

Figure 4. Normalised squared moduli of exciton wave functions calculated from $\mathbf{k}\cdot\mathbf{p}$ model for (a) ML and (b) BL $MoSe_2$. Dispersions of exciton *g*-factors around K^+ point from DFT calculations for (c) ML and (d) BL.

The resulting trends of the calculated *g*-factors are in good agreement with the experimental values, as presented in table 1. Particularly, the experimentally observed large increase of the *g*-factors of $2s^A$ excitons in ML and BL can not be explained either by the underestimation of the band gap by DFT [49], or by the in-plane mechanical strain that might be present in the samples [51]. Further theoretical investigations are required, which are beyond the scope of this study.

5. Summary

The excitonic properties in high-quality ML and BL of molybdenum diselenide ($MoSe_2$) encapsulated in hBN flakes were investigated both theoretically and experimentally. We determined the *g*-factors of the intralayer A and B excitons and of the interlayer excitons in $MoSe_2$ ML and BL using the RC experiment performed in out-of-plane magnetic fields up to 10 T and first-principle calculations. The experimental ladder of excitonic *s* states in the ML was reproduced using the $\mathbf{k}\cdot\mathbf{p}$ model with the Rytova–Keldysh potential. Furthermore, we demonstrated that analogous calculations for the BL require taking into account the out-of-plane dielectric response of the $MoSe_2$ BL, which is neglected for the ML. Finally, we have explained the values and signs of all observed

g-factors using a combined $\mathbf{k}\cdot\mathbf{p}$ and DFT approach. Our results manifest that the excitonic physics in S-TMD BLs is more complex than that in the ML case because of the presence of VB hybridization and the non-infinite size of the BL.

6. Methods

6.1. Sample and experimental setup

The investigated $MoSe_2$ thin layers and hBN flakes were fabricated by two-stage PDMS-based mechanical exfoliation of the bulk crystal. Initially, the hBN thin flakes were exfoliated onto a 90 nm SiO_2/Si substrate and annealed at 200 °C. That non-deterministic approach provides the best quality of the substrate surface. Subsequent layers were transferred deterministically using a microscopic system equipped with a x-y-z motorised positioners. The assembled structures were annealed at 160 °C for 1.5 hour in order to ensure the best layer-to-layer and layer-to-substrate adhesion and to eliminate a substantial portion of air pockets apparent at the interfaces between the constituent layers.

Low-temperature micro-magneto-experiments of RC were performed in Faraday geometry, i.e. magnetic field oriented perpendicularly to the layers plane. Measurements (spatial resolution $\sim 3\,\mu$m) were carried out with the aid of a superconducting coil in magnetic fields up to 10 T using an optical fibre arrangement. The sample was placed on top of a x-y-z piezo-stage kept at $T = 10$ K and was illuminated using a 100 W tungsten halogen lamp. The reflectance signal was dispersed with a 0.75 m focal length monochromator and detected with a liquid-nitrogen-cooled Si-CCD. The combination of a quarter-wave plate, a linear polariser, and a Wollastom prism was used to analyse the circular polarisation of signals (the $\sigma^{\pm}$-polarized light was measured simultaneously). We define the RC spectrum as $\mathrm{RC}(E) = [\mathrm{R}(E) - \mathrm{R}_0(E)]/[\mathrm{R}(E) + \mathrm{R}_0(E)] \times 100\%$, where $\mathrm{R}(E)$ and $\mathrm{R}_0(E)$ are the reflectance of the sample and of the same structure without the ML or BL of $MoSe_2$, respectively.

6.2. DFT calculations

First-principles calculations within the DFT were carried out in the Vienna ab-initio simulation package [52]. The ionic potentials were described using the projector augmented wave technique [53]. We employed the generalised gradient approximation of the exchange correlation-functional within Perdew–Burke–Ernzerhof parametrization [54]. A cut-off energy for the plane-wave basis and a Monkhorst-Pack k-grid for the BZ sampling were set to 500 eV and $12 \times 12 \times 1$, respectively. The geometrical structures of ML and BL were defined using the parameters from [46] with a vacuum region of 20 Å in order to avoid spurious interactions between the periodically repeated layers. Spin–orbit coupling was taken into account during the calculations.

Data availability statement

The data cannot be made publicly available upon publication because they are not available in a format that is sufficiently accessible or reusable by other researchers. The data that support the findings of this study are available upon reasonable request from the authors.

Acknowledgment

We thank Paulo E Faria Junior for fruitful discussions. The work has been supported by the National Science Centre, Poland (Grant No. 2017/27/B/ST3/00205 and 2018/31/B/ST3/02111). A O S acknowledges the support by Czech Science Foundation (project GA23-06369S). T W acknowledges support from the National Science Centre, Poland (Grant No. 2021/41/N/ST3/04516). K W and T T acknowledge support from JSPS KAKENHI (Grant Numbers 19H05790, 20H00354 and 21H05233). DFT calculations were performed with the support of Center for Information Services and High Performance Computing (ZIH) at TU Dresden and in part by PLGrid Infrastructure.

Author Contributions

Ł K, M B, N Z, K O-P, A B, and M R M performed the experiments. A O S performed theoretical calculations based on the $\mathbf{k}\cdot\mathbf{p}$ approximation. T W carried out DFT calculations. M G fabricated the sample K W and T T grew the hBN crystals. M R M supervised the project. Ł K, A O S, T W, and M R M wrote the manuscript with inputs from the all co-authors.

Conflict of interest

There are no conflicts to declare.

ORCID iDs

Łucja Kipczak https://orcid.org/0000-0003-1266-0201
Artur O Slobodeniuk https://orcid.org/0000-0001-5798-0431
Tomasz Woźniak https://orcid.org/0000-0002-2290-5738
Mukul Bhatnagar https://orcid.org/0000-0003-3712-371X
Natalia Zawadzka https://orcid.org/0000-0002-3282-9513
Katarzyna Olkowska-Pucko https://orcid.org/0000-0002-6036-7096
Magdalena Grzeszczyk https://orcid.org/0000-0001-6861-3098

Kenji Watanabe https://orcid.org/0000-0003-3701-8119
Takashi Taniguchi https://orcid.org/0000-0002-1467-3105
Adam Babiński https://orcid.org/0000-0002-5591-4825
Maciej R Molas https://orcid.org/0000-0002-5516-9415

References

[1] Mak K F, Lee C, Hone J, Shan J and Heinz T F 2010 *Phys. Rev. Lett.* **105** 136805
[2] Arora A, Koperski M, Nogajewski K, Marcus J, Faugeras C and Potemski M 2015 *Nanoscale* **7** 10421
[3] Arora A, Nogajewski K, Molas M, Koperski M and Potemski M 2015 *Nanoscale* **7** 20769
[4] Molas M R, Nogajewski K, Slobodeniuk A O, Binder J, Bartos M and Potemski M 2017 *Nanoscale* **9** 13128
[5] Chernikov A, Berkelbach T C, Hill H M, Rigosi A, Li Y, Aslan O B, Reichman D R, Hybertsen M S and Heinz T F 2014 *Phys. Rev. Lett.* **113** 076802
[6] Koperski M, Molas M R, Arora A, Nogajewski K, Slobodeniuk A O, Faugeras C and Potemski M 2017 *Nanophotonics* **6** 1289
[7] Wang G, Chernikov A, Glazov M M, Heinz T F, Marie X, Amand T and Urbaszek B 2018 *Rev. Mod. Phys.* **90** 021001
[8] Molas M R, Slobodeniuk A O, Nogajewski K, Bartos M, Bala L, Babiński A, Watanabe K, Taniguchi T, Faugeras C and Potemski M 2019 *Phys. Rev. Lett.* **123** 136801
[9] Goryca M *et al* 2019 *Nat. Commun.* **10** 4172
[10] MacDonald A H and Ritchie D S 1986 *Phys. Rev.* B **33** 8336
[11] Koteles E S and Chi J Y 1988 *Phys. Rev.* B **37** 6332
[12] Rytova N S 1967 *Mosc. Univ. Phys. Bull.* **3** 30
[13] Keldysh L V 1979 *JETP Lett.* **29** 716
[14] Fang S, Kuate Defo R, Shirodkar S N, Lieu S, Tritsaris G A and Kaxiras E 2015 *Phys. Rev.* B **92** 205108
[15] Sun Y, Wang D and Shuai Z 2016 *J. Phys. Chem.* C **120** 21866
[16] Ruiz-Tijerina D A, Danovich M, Yelgel C, Zólyomi V and Fal'ko V I 2018 *Phys. Rev.* B **98** 035411
[17] Slobodeniuk A O *et al* 2019 *2D Mater.* **6** 025026
[18] Leisgang N *et al* 2020 *Nat. Nanotechnol.* **15** 901
[19] Horng J, Stroucken T, Zhang L, Paik E Y, Deng H and Koch S W 2018 *Phys. Rev.* B **97** 241404
[20] Paradisanos I *et al* 2020 *Nat. Commun.* **11** 2391
[21] Das S, Dandu M, Gupta G, Murali K, Abraham N, Kallatt S, Watanabe K, Taniguchi T and Majumdar K 2020 *ACS Photonics* **7** 3386
[22] Lorchat E, Selig M, Katsch F, Yumigeta K, Tongay S, Knorr A, Schneider C and Höfling S 2021 *Phys. Rev. Lett.* **126** 037401
[23] Zhao Y *et al* 2022 *Phys. Rev.* B **105** L041411
[24] Altaiary M M, Liu E, Liang C-T, Hsiao F-C, van Baren J, Taniguchi T, Watanabe K, Gabor N M, Chang Y-C and Lui C H 2022 *Nano Lett.* **22** 1829
[25] Hagel J, Brem S and Malic E 2022 *2D Mater.* **10** 014013
[26] Feng S, Campbell A, Brotons-Gisbert M, Baek H, Watanabe K, Taniguchi T, Urbaszek B, Gerber I C and Gerardot B D 2022 arxiv:2212.14338
[27] Koperski M, Molas M R, Arora A, Nogajewski K, Bartos M, Wyzula J, Vaclavkova D, Kossacki P and Potemski M 2019 *2D Mater.* **6** 015001
[28] Arora A, Koperski M, Slobodeniuk A, Nogajewski K, Schmidt R, Schneider R, Molas M R, de Vasconcellos S M, Bratschitsch R and Potemski M 2018 *2D Mater.* **6** 015010
[29] Liu E, van Baren J, Liang C-T, Taniguchi T, Watanabe K, Gabor N M, Chang Y-C and Lui C H 2020 *Phys. Rev. Lett.* **124** 196802
[30] He M *et al* 2020 *Nat. Commun.* **11** 618
[31] Zinkiewicz M *et al* 2021 *Nano Lett.* **21** 2519
[32] Pucko K O *et al* 2022 *2D Mater.* **10** 015018
[33] Li Y *et al* 2014 *Phys. Rev. Lett.* **113** 266804
[34] Xiao K, Yan T, Liu Q, Yang S, Kan C, Duan R, Liu Z and Cui X 2021 *J. Phys. Chem. Lett.* **12** 2555
[35] Stier A V, Wilson N P, Clark G, Xu X and Crooker S A 2016 *Nano Lett.* **16** 7054
[36] Chen S-Y *et al* 2019 *Nano Lett.* **19** 2464
[37] Delhomme A *et al* 2019 *Appl. Phys. Lett.* **114** 232104
[38] Raiber S, Faria Junior P E, Falter D, Feldl S, Marzena P, Watanabe K, Taniguchi T, Fabian J and Schüller C 2022 *Nat. Commun.* **13** 4997
[39] Gerber I C *et al* 2019 *Phys. Rev.* B **99** 035443
[40] Grzeszczyk M *et al* 2021 *Sci. Rep.* **11** 17037
[41] Cudazzo P, Tokatly I V and Rubio A 2011 *Phys. Rev.* B **84** 085406
[42] Kormányos A, Burkard G, Gmitra M, Fabian V, Zólyomi J, Drummond V and Fal'ko N D 2015 *2D Mater.* **2** 022001
[43] Gong Z, Liu G-B, Yu H, Xiao D, Cui X, Xu X and Yao W 2013 *Nat. Commun.* **4** 2053
[44] Slobodeniuk A O, Koutenský P, Bartoš M, Trojánek F, Malý P, Novotný T and Kozák M 2022 *Phys. Rev.* B **106** 235304
[45] Wannier G H 1937 *Phys. Rev.* **52** 191
[46] Berkelbach T C, Hybertsen M S and Reichman D R 2013 *Phys. Rev.* B **88** 045318
[47] Geick R, Perry C H and Rupprecht G 1966 *Phys. Rev.* **146** 543
[48] Laturia, A, Van de Put M L and Vandenberghe W G 2018 *npj 2D Mater. Appl.* **2** 6
[49] Woźniak T, Faria Junior P E, Seifert G, Chaves A and Kunstmann J 2020 *Phys. Rev.* B **101** 235408
[50] Gajdoš M, Hummer K, Kresse G, Furthmüller J and Bechstedt F 2006 *Phys. Rev.* B **73** 045112
[51] Junior P E F, Zollner K, Woźniak T, Kurpas M, Gmitra M and Fabian J 2022 *New J. Phys.* **24** 083004
[52] Kresse G and Furthmüller J 1996 *Phys. Rev.* B **54** 11169
[53] Kresse G and Joubert D 1999 *Phys. Rev.* B **59** 1758
[54] Perdew J P, Burke K and Ernzerhof M 1996 *Phys. Rev. Lett.* **77** 3865